C. R. Physique 15 (2014) 214–223

Contents lists available at ScienceDirect

Comptes Rendus Physique

www.sciencedirect.com

Electron microscopy / Microscopie électronique

Liquid scanning transmission electron microscopy: Nanoscale imaging in micrometers-thick liquids

Microscopie électronique à balayage en transmission en phase liquide : Imager à l'échelle du nanomètre à travers des films liquides de plusieurs micromètres d'épaisseur

Tobias Schuh, Niels de Jonge *

INM – Leibniz Institute for New Materials, Campus D2 2, 66123 Saarbrücken, Germany

ARTICLE INFO

Article history:
Available online 24 January 2014

Keywords:
STEM
Liquid specimen
Resolution theory
Eukaryotic cell
Gold nanoparticle
Time-lapse STEM

Mots-clés :
STEM
Échantillon liquide
Théorie de la résolution
Cellule eukaryote
Nanoparticule d'or
STEM résolue en temps

ABSTRACT

Scanning transmission electron microscopy (STEM) of specimens in liquid is possible using a microfluidic chamber with thin silicon nitride windows. This paper includes an analytic equation of the resolution as a function of the sample thickness and the vertical position of an object in the liquid. The equipment for STEM of liquid specimen is briefly described. STEM provides nanometer resolution in micrometer-thick liquid layers with relevance for both biological research and materials science. Using this technique, we investigated tagged proteins in whole eukaryotic cells, and gold nanoparticles in liquid with time-lapse image series. Possibly future applications are discussed.

RÉSUMÉ

La microscopie électronique à balayage en transmission (STEM) d'échantillons immergés dans un liquide est possible en utilisant une chambre microfluidique réalisée avec de fines fenêtres en nitrure de silicium. Cet article introduit d'abord une équation analytique permettant d'estimer la résolution spatiale accessible en fonction de l'épaisseur totale de l'échantillon et de la position de l'objet d'intérêt en son sein. Après une description brève de l'équipement utilisable, nous montrons comment cette approche STEM permet d'observer avec une résolution nanométrique des objets d'intérêt en biologie ou en science des matériaux, plongés dans une couche liquide de plusieurs micromètres d'épaisseur. Avec cette technique, nous avons étudié la distribution de protéines marquées dans des cellules eucaryotes complètes et celle dynamique de nanoparticules d'or dans un liquide au moyen de séries d'images résolues en temps. Enfin, nous proposons quelques grands axes pour de futures applications.

* Corresponding author.
E-mail address: niels.dejonge@inm-gmbh.de (N. de Jonge).

1631-0705/$ – see front matter
http://dx.doi.org/10.1016/j.crhy.2013.11.004

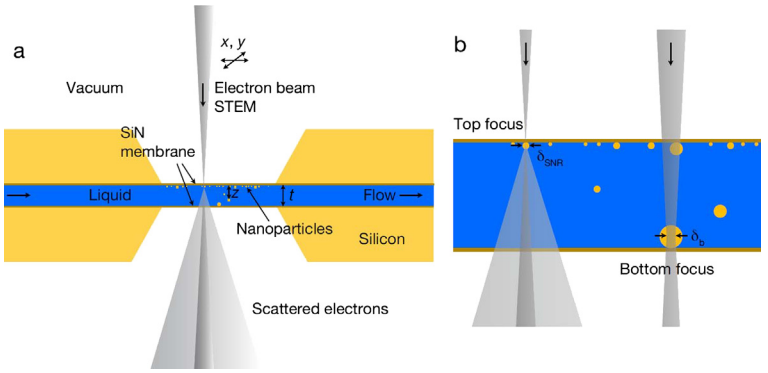

Fig. 1. (Color online.) Principle of scanning transmission electron microscopy (STEM) of specimens in liquid, termed Liquid STEM. (a) A microfluidic chamber is formed between two silicon nitride (SiN) membranes supported on silicon microchips. A sample, for example, containing nanoparticles is placed within a liquid layer of thickness t. The vertical distance from the beam entrance is referred to as z. Imaging is accomplished by scanning a focused electron beam over the sample. Elastically scattered and transmitted electrons are recorded with the annular dark field detector located beneath the sample. (b) Close-up of the impact of the focused electron beam with the sample for the case when focusing at the top layer of the liquid (left). The resolution δ_{SNR} is limited by noise and given by the diameter of the smallest visible object. The probe size of the focused electron beam may be smaller than δ_{SNR}. In the case when focusing at the bottom, scattering leads to a broadening of the electron beam (right). In the latter case, the resolution is limited by the size of the broadened electron probe δ_b.

1. Introduction

Electron microscopy traditionally studies solid samples in the vacuum chamber of the microscope. But for many research questions, it is desired to image specimens in a liquid environment, for example, for the study of colloidal assembly, catalyst particles, growth of nanomaterials, energy materials, and biological cells and macromolecules [1]. Already since the early days of electron microscopy, systems were discussed to study nanoparticles or biological cells in a wet environment [2,3]. Various systems for transmission electron microscopy (TEM) have been developed over the years [4,5], eventually leading to the achievement of atomic resolution in thin liquid layers [6–8]. A drawback of liquid-cell TEM remains that nanoscale resolution cannot be obtained for liquid thicknesses of more than several hundreds of nanometers on account of scattering of the electron beam in the liquid layer [1]. For several studies, it is required, however, to achieve high resolution in several micrometer thick liquid layers. Such thicknesses are needed, for example, for imaging eukaryotic cells, for imaging micrometer-sized objects relevant for energy storage and conversion, or to achieve a continuous liquid flow. One option to study more bulky samples in a liquid is to use environmental scanning electron microscopy (SEM) [9–11] or dedicated liquid specimen systems for SEM [12,13]. However, nanometer resolution can be reached only at or close to the surface or in very thin samples. A new approach was introduced combining scanning transmission electron microscopy (STEM) with the usage of silicon nitride (SiN) membranes as windows in a liquid compartment [14]. This so-called Liquid STEM approach can image nanoscale materials of high atomic number (Z) in low-Z liquids, resulting from the Z contrast of STEM [15–18]. For example, gold nanoparticles (AuNPs) can be imaged in a micrometer-thick liquid water layer within a microfluidic chamber [19,20], see Fig. 1. Additionally, liquid STEM can be used to study the distribution of a certain protein species in whole cells using AuNPs as specific labels [21], similar as proteins tagged with fluorescent labels are used for fluorescence microscopy [22], but then with a factor of 50-fold higher resolution. STEM of liquid specimens was also used in materials science, for example, to study the growth of Pb nanoparticles in solution with atomic resolution [23], to image the dynamic movement of AuNPs in liquid [24,25], and even electron energy loss spectroscopy in liquid layers has proven feasible [26,27]. In case STEM is used for thin liquid layers, lower Z materials are also visible with nanoscale resolution, for example macromolecular protein complexes [28]. In this paper we will provide the theoretical concepts behind Liquid STEM, describe the key components of the instruments, and discuss examples of its usage in both biology and materials science.

2. Theory

STEM produces (sub-)nanometer-resolution images by scanning a focused electron beam over a thin sample [15]. Electrons transmitted from the top through the sample and scattered outside the cone of the primary electron beam are detected with an annular dark field (ADF) detector [17]. The Z-contrast of STEM images is dominated by elastic scattering of the electrons at the core of the atoms in the specimen. The number of inelastic scattering events is actually higher for some samples, but they mainly involve small-angle scattering, and can often be neglected when calculating the signal in the ADF detector [17]. Yet, inelastic scattering needs to be taken into account mainly for beam broadening (discussed later in the text) and its influence on the specimen via radiation damage.

The number $N(t)$ of elastically scattered electrons in the ADF detector increases with the sample thickness t and decreases with the mean free path length $l(E, \beta, Z)$ of the electron in the sample [17,18]:

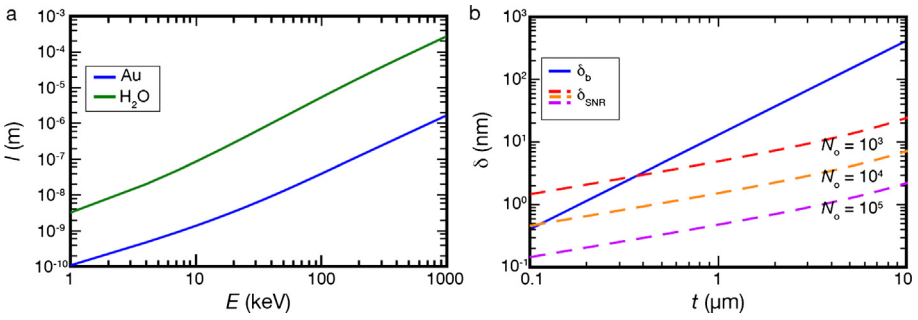

Fig. 2. (Color online.) Calculating the spatial resolution of Liquid STEM. (a) Mean free path length l as a function of the electron energy E for a layer of water, and gold. The values of l were calculated for acceptance semi-angle $\beta = 94$ mrad, and electron energy $E = 200$ keV, such that $l_{\text{gold}} = 121$ nm, and $l_{\text{water}} = 18.5$ μm. (b) The noise-limited resolution δ_{SNR} and the beam-broadening-limited resolution δ_{b} plotted as a function of the water thickness t for different numbers of electrons per pixel ($N_0 = 1000$; 10,000, and 100,000).

$$N(t) = N_0\left(1 - \exp\left(-\frac{t}{l(E,\beta,Z)}\right)\right) \tag{1}$$

with N_0 the number of incident electrons per pixel. In this model, it is assumed that the contrast-forming event is a single electron scattering event, after which the electron travels towards the detector. The contrast may be reduced by a second scattering event (or more) changing the direction of the electron away from the opening of the detector. But even though additional scattering events are likely to occur in thicker samples, most scattering occurs in a narrow-angle range and only a minor chance exists that the angle is changed to such extent that detection does not occur. Indeed, for water thicknesses of under 10 μm, the model agrees with experimental data and also with Monte Carlo simulations [20]. The contrast eventually vanishes for larger (mass) thicknesses. The mean free path length depends on the scattering cross-section σ [17], a function of Z, the beam energy E, and the detector acceptance semi-angle β of the ADF detector (inner angle of annular detector), so that the cross-section corresponds to scattering to angles larger than β.

$$l(E,\beta,Z) = \frac{W}{\sigma(E,\beta,Z)\rho N_{\text{A}}} \tag{2}$$

with the material properties (mass density ρ and atomic weight W), and Avogadro's number N_{A}.

In the general case of a material consisting of different atoms, the average elastic cross-section is calculated by summing all the cross-sections of all atoms present and dividing by the total number of atoms [18]. For materials containing different concentrations of atom species, the average cross-section can be used [29], $\langle\sigma\rangle = \sum p_i\sigma_i$ with p_i the concentration of atom i in the material. The average mean free path $\langle l\rangle$ can then be calculated

$$\langle l\rangle = \frac{\langle W\rangle}{N_{\text{A}}\rho\langle\sigma\rangle} \tag{3}$$

with the average atomic number $\langle W\rangle = \sum p_i W_i$.

The influence of the electron energy E to l is plotted for gold and water in Fig. 2a. The strong dependence of σ on Z results in the so-called Z-contrast, which makes it possible to detect heavy nanoparticles of, for example, gold within a micrometer-thick layer consisting of water or other light elements. The cross-section of water is approximately two orders of magnitude smaller than that of gold, and, therefore, the Au mean free path is much smaller. Fig. 2a exemplifies that a gold layer of several tens of nanometers thickness scatters the same amount of electrons into the ADF detector as a water layer of several micrometers thickness.

When imaging a round object of diameter d in the top layer of the liquid with respect to a downward traveling electron beam (left-hand side situation in Fig. 1b), the resolution is typically noise limited [20]. The contrast is formed from the signal difference between a pixel recorded at the position of the object and a pixel in which the electron beam interacts with the liquid only [17,19,20]. The object can be detected if the signal from a pixel containing the object is at least five times larger than the background signal from the surrounding liquid, following the Rose criterion [30]. The background exhibits statistical fluctuations (Poisson distribution) considered as background noise in the experiment. It was experimentally verified that the minimum detectable size d_{min} can be used as measure of the spatial resolution δ_{SNR} in lateral direction [20]. The resolution can be calculated starting at the signal-to-noise ratio SNR:

$$SNR = \frac{N_{\text{s}} - N_{\text{b}}}{\sqrt{N_{\text{b}}}} = 5 \tag{4}$$

The signal N_{s} is calculated using Eq. (1) from a pixel containing the object of height d and the liquid layer of height $t - d$ [19,20],

$$N_{\text{s}} = N_0\left[1 - \exp\left\{-\left(\frac{d}{l_{\text{o}}} + \frac{t-d}{l_{\text{l}}}\right)\right\}\right] \tag{5}$$

and the background signal N_b reflecting scattering in a liquid layer of height t:

$$N_b = N_0\left[1 - \exp\left\{-\frac{t}{l_l}\right\}\right] \tag{6}$$

with l_o and l_l the mean free path of the object and the liquid, respectively. Solving Eq. (4) for d_{min} using Eqs. (5) and (6) leads to the complete analytic solution:

$$\delta_{SNR} = d_{min} = \frac{l_l l_o}{l_o - l_l}\left(\ln\left\{-5\sqrt{1/N_0\left[1 - \exp\left(-\frac{t}{l_l}\right)\right]} + \exp\left(-\frac{t}{l_l}\right)\right\} + \frac{t}{l_l}\right) \tag{7}$$

The dependence of the resolution δ_{SNR} on the sample thickness t is plotted in Fig. 2b for different amounts of electrons per pixel. The equation was found to agree well with previously published experimental data and the numerical solution [20]. It can be seen that Liquid STEM provides nanoscale resolution for liquid thickness of several micrometers but also atomic resolution of 0.2 nm for $t < 0.2$ µm ($N_0 = 10^5$). That it is possible to achieve atomic resolution with STEM in liquid was demonstrated by others for lead dioxide nanoparticles in water [26]. Eq. (7) also holds for amorphous solid or gaseous samples. But it should be noted that the equation is a simple model only. The point spread function of the electron beam and diffraction effects are not included, and a perfect detector is assumed. Furthermore, one typically adjusts the pixel size such that the objects of interest are scanned with a multiple of pixels. In the latter case, the Rose criterion, based on the detection of one pixel, could principally be relaxed. Similarly, different statistical considerations have to be made for the imaging of non-round objects, for example, tubes, where the smallest observable diameter will probably be smaller than δ_{SNR}.

For the typical case of the detection of gold or platinum nanoparticles in a liquid layer ranging in thickness up to 5 µm, Eq. (7) can be approximated with an accuracy of a factor of two by the following expression [19,20]:

$$\delta_{SNR} \approx 5 l_o \sqrt{\frac{t}{N_0 l_l}} \tag{8}$$

This expression can be used for quick estimates of the achievable resolution as a function of the number of electrons per pixel. The same model can also be used for other types of materials, but if they differ greatly in Z from gold and water, the validity of the approximations needs to be checked using the full Eq. (2).

For the imaging of NPs at the bottom of the liquid (right-hand side situation in Fig. 1b), the STEM spot is focused at the bottom layer but scattering of the electron beam in the liquid broadens the spot. The resolution δ_b is typically limited by beam broadening of the electron beam in the micrometers-thick liquid layer t_a above the object of interest and can be calculated from the 25–75% edge width [17]:

$$\delta_b = \frac{\lambda^2}{2\pi a_H} t_a^{3/2} \sqrt{\frac{N_A \rho}{3\pi W}} Z\left(1 + \frac{E}{m_0 c^2}\right), \quad \text{with } \lambda = \frac{hc}{\sqrt{2Em_0c^2 + E^2}} \tag{9}$$

Here, a_H is the Bohr radius, m_0 the mass of an electron, c the speed of light, and h the Planck constant. The parameters ρ, Z, and W are those of the liquid [20,31]. The strong dependence on the thickness of the liquid is exemplified in Fig. 2b. This model of beam broadening includes also multiple scattering events. Eq. (9) is similar to the diameter of the broadened beam containing 25% of the current [20]. Others have also concluded that nanometer-sized gold particles can be resolved below thick low-Z specimens, and found similar expressions for the beam broadening but then for the case of solid specimens [32–34]. For completeness, it should be noted that Eq. (9) might not always be a reliable measure of the resolution for very thin layers. When only a minimal degree of blurring is present, the objects can still be imaged with the high-resolution point spread function of the electron probe, while broadening merely adds to an increased noise level, or the so-called beam tails. It was shown in the example of a thick carbon layer that the probe size measured from the full width at half maximum was indeed smaller than predicted by Eq. (9) [35].

After having described the resolution on the top and at the bottom of the liquid layer, the question remains to know how the resolution changes depending on the depth z of the object in the liquid. Two effects have to be considered in parallel, since the resolution depends differently on the liquid thickness. δ_{SNR} is essentially not sensitive to the depth of the object in the liquid, only to the total thickness of the liquid layer because the background signal results from scattering in the entire liquid layer. In contrast, δ_b is affected by the thickness of the liquid above the object, but we do not need to consider the liquid below the object, such that $\delta_b(t) = \delta_b(z)$. The number of electrons per pixel necessary to detect an object of dimensions δ_{SNR} is sufficient to detect the object deeper in the liquid. Both cases are plotted in Fig. 3a. The two resolution measures are independent, and can thus be convoluted to a resolution depending on the depth in the water z and the thickness t of the liquid:

$$\delta(z,t) = \sqrt{\delta_{SNR}^2(t) + \delta_b^2} \tag{10}$$

Combining both resolution measures, we can state that δ_{SNR} is larger, i.e. dominating, at small thicknesses, while δ_b becomes larger beyond a certain thickness. In Fig. 3a, the resolution $\delta(z,t)$ approaches δ_{SNR} for positions close to the top

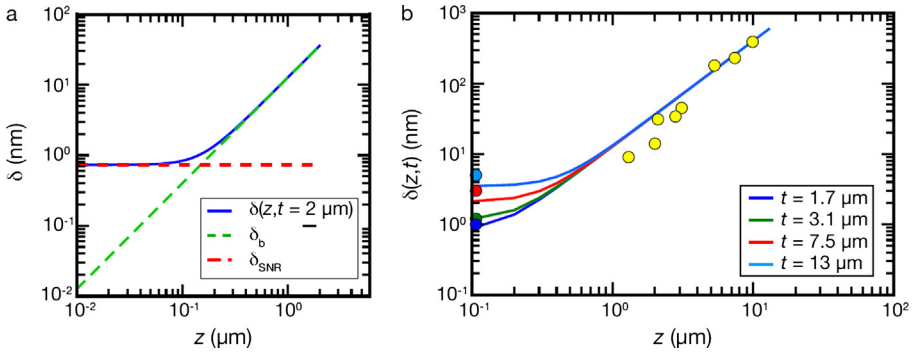

Fig. 3. Calculation of the resolution as a function of the vertical position within the liquid (z). (a) The calculated resolution $\delta(t, z)$ depending on the depth z of an AuNP in a 2-μm-thick water layer (blue line). The calculations were conducted for $E = 200$ keV, $\beta = 94$ mrad, and 6.6×10^4 electrons. The δ_{SNR} for an AuNP at the top of a liquid layer as a function of the liquid thickness is shown as a red dashed line. The resolution δ_b for an AuNP at depth z in the liquid is shown as a green dashed line. (b) The $\delta(t, z)$ for different water thicknesses are compared to experimental data. The data for AuNPs at the top of the liquid are shown as blue, green, red, and light blue dots for $t = 1.7$ μm, 3.1 μm, 7.5 μm, and 13.5 μm, respectively. Data at the bottom of the liquid (yellow dots) were used as measures of δ_b setting $t = z$. (For interpretation of the references to color in this figure legend, the reader is referred to the web version of this article.)

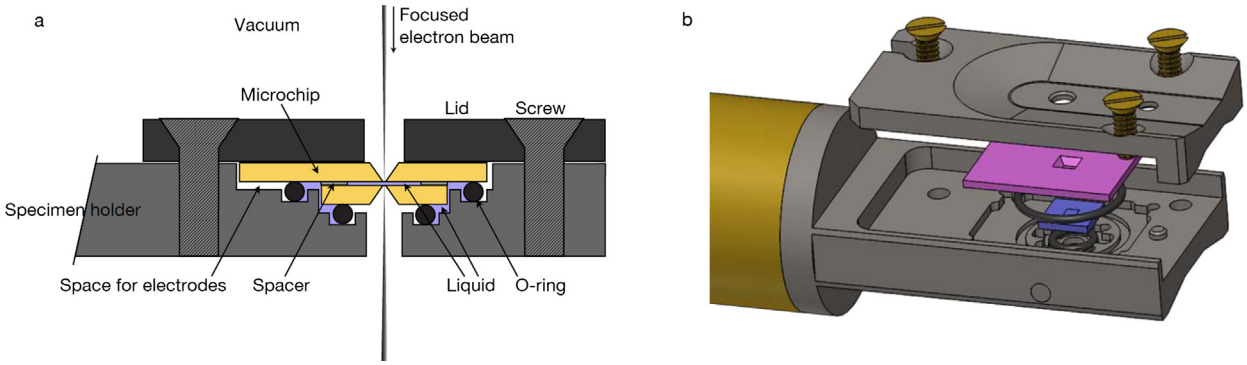

Fig. 4. (Color online.) Schematics of the tip of the liquid flow specimen holder. (a) Two microchips supporting thin silicon nitride (SiN) windows are placed in the liquid compartment on the tip of the liquid flow specimen holder. Two O-rings provide vacuum sealing and are compressed by closing a lid with screws. (b) Three-dimensional drawing of the tip showing the loading of the microchips. The liquid flows from a port at the short side of the microchips between and along the window to another port at the opposite side.

window. At approximately 1-μm depth, the resolution becomes dominated by beam broadening δ_b. The highest resolution is obtained for nanoparticles in the top layer of the liquid for STEM, while the lowest resolution is obtained at the bottom. This trend is the opposite of the TEM case, where the highest resolution is obtained at the bottom of the liquid layer [1,8], in accordance with the principle of reciprocity theorem [17].

To verify the aforementioned model, it was compared with previously published experimental data [20] in which the resolution values of AuNPs on the top and at the bottom of the water layer were determined for different water thicknesses. The experiments were conducted at $E = 200$ keV, $\beta = 94$ mrad, and $N_0 = 6.6 \times 10^4$ electrons. The results of the measurement in the top water layer are shown in Fig. 3b as dots at the left axis. The resolution on top of the water layer is slightly underestimated by the assumed model compared to the experimental data for larger values of t. The yellow dots represent the experimental resolution below the water. To compare the experimental data recorded below liquid layers with the calculated resolution, we assumed $t = z$, i.e. the experimental resolution was plotted as a function of z, while it was measured as a function of t. Nevertheless, the resolution in the range of the measurements shows a reasonably good agreement with our experimental data. The simple model of Eq. (10) serves as a guide to design and interpret experiments. If needed, the achievable resolution can be calculated with more precision as a function of the 3D sample geometry and for any location within the sample using Monte Carlo calculations calibrated for STEM imaging, including the noise of the electron source [20,35,36].

3. Instrumentation

The main component for Liquid STEM is a silicon microchip supporting a thin and electron-transparent silicon nitride (SiN) window (Protochips, Inc., NC) [14,37]. Two microchips are placed on the tip of a specimen holder for liquid flow (Protochips Inc., NC). Schematic drawings are shown in Fig. 4. The design involves a larger and a smaller microchip, and two O-rings. The thinnest region of the tip fits within 1.4 mm as needed for the ultra-high resolution pole piece of the ARM200

Fig. 5. (Color online.) Liquid flow specimen TEM/STEM holder system ("Poseidon" Protochips Inc., NC., USA). Microchips in a box are shown at the left lower corner. A microfluidic syringe pump is connected with the holder via plastic tubing.

STEM/TEM (JEOL). The liquid compartment is connected to the exterior through liquid tubing in the shaft of the holder. A microfluidic syringe pump (Harvard Apparatus) drives the liquid flow through the holder. A photograph of the system is shown in Fig. 5. The liquid flow specimen holder system consists of only three elements (the microfluidic chamber formed by a large and a small microchip, the specimen holder, and the pump with syringe), transforming a standard electron microscope into a system for imaging specimens in liquid. The system can be used for either TEM or STEM, each achieving the highest resolution for different liquid thicknesses [1,8,20]. Note that the same system can also be used for *in situ* electron microscopy of specimens in gaseous environments at atmospheric pressure [38].

A SiN membrane thickness of 50 nm is typically used for application with liquid thickness of several micrometers. This thickness provides a strong membrane that is not too fragile, while it is sufficiently thin compared to the involved liquid thickness of several micrometers, such that the interaction of the electron beam with the window can be neglected [20, 37]. A rectangular shape of the window of typically 50×400 μm^2 can be used. This shape balances a maximal field of view with the largest strength and stiffness. Bulging occurs when the microfluidic chamber is placed in the vacuum of the electron microscope, amounting to about 1 μm per window for the above dimensions [20,39]. A smaller degree of bulging can be obtained by reducing the short dimension of the window. The sides of the microchips were manufactured with a precision of ± 10 μm with respect to the SiN window position, in order to allow precise alignment of the windows when the two microchips are stacked as needed for transmission electron microscopy. Nevertheless alignment may be difficult to achieve for windows smaller than 50 μm and microchips with crossed windows (not parallel) are available to avoid the alignment problem. One of the microchips contains a spacer [37], of a desired thickness (0.5–5 μm), such that the liquid can flow between the microchips, and to provide a specimen chamber with sufficient height. Liquid thicknesses in the range of several micrometers [20] to hundreds of nanometers are readily achieved [27].

The Liquid STEM system can also be used for correlative light microscopy and Liquid STEM, which is of relevance for the study of various biological questions. The simplest approach is to image a microchip with cells first with light microscopy, to subsequently assemble the microchip in the microfluidic device, and to image the enclosed specimen with Liquid STEM [40,41]. But live or fixed cells can also be assembled right way in the microfluidic device on the tip of the specimen holder. The holder can then be placed on the objective lens of an inverted light microscope, and imaged with Liquid STEM directly thereafter [42].

4. Liquid STEM of whole eukaryotic cells

One application area of the Liquid STEM is for the study of eukaryotic cells. Initial experiments involved COS7 fibroblast cells [19]. They were grown directly on microchips coated with poly-L-lysine to promote cell adherence [41]. The aim of the experiments was to visualize the location of the epidermal growth factor receptor (EGFR). The EGFR is a transmembrane receptor [43] playing a critical role in the pathogenesis and progression of several types of cancer [44]. For this purpose, the cells were incubated with the receptor ligand (EGF) conjugated to AuNPs of 10 nm of diameter. A microchip with labeled COS7 cells was assembled into a microfluidic device by placing it on the tip of the liquid flow specimen holder while keeping it wet. A second microchip with spacer (typically 5 μm) was then placed on the tip with the SiN side facing down. The lid was closed, and liquid flow of a 10% phosphate buffered solution in water was initiated. The liquid flow served to test the system for leakage prior to electron microscopic imaging. The cells were firmly adhering to the SiN membrane and did not move in the liquid flow.

A CM200 STEM/TEM (Philips, FEI) was used for imaging with the following settings: electron probe convergence angle $\alpha = 5$ mrad, dwell time $\tau = 20$ μs, $\beta = 70$ mrad, probe current $I = 0.5$ nA, and $E = 200$ keV. The image size was 1024×1024 pixels, leading to an image acquisition time of 20 s. Fig. 6a shows the edge of a COS7 fibroblast cell that was incubated for

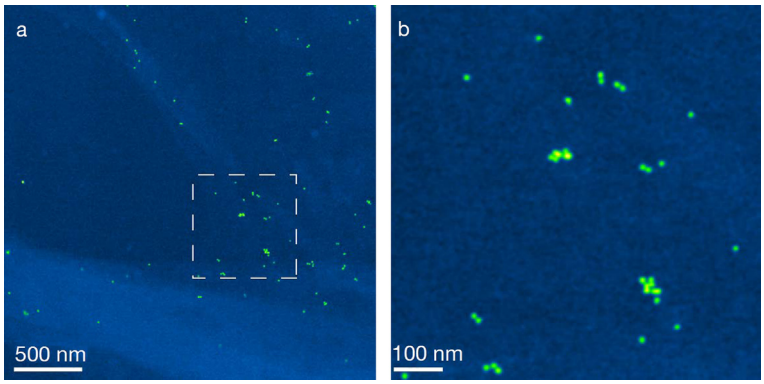

Fig. 6. Liquid STEM of whole fixed COS7 cells in a liquid. Epidermal growth factor receptors were labeled with gold nanoparticles (AuNPs). (a) Image at the edge of the cell. AuNPs are visible as yellow spots and the cellular material as light-blue material over the dark-blue background. (b) Magnified image of the region in an indicated with the dashed rectangle. The individual AuNPs are clearly visible. Image with permission from [19] modified with color added. (For interpretation of the references to color in this figure legend, the reader is referred to the web version of this article.)

5 min with 10-nm-diameter AuNPs conjugated with EGF. The measured spatial resolution was 4 nm, which was sufficient to distinguish between single labels, dimers, or larger clusters, as can be seen in Fig. 6b. Importantly, the resolution obtained on the sample in the liquid was not spoiled by motion of the structure under observation [19,45]. The cellular material was visible at a lower resolution as light blue shapes. It is not possible with any other microscopy technique to directly image the locations of labels with nanometer resolution on whole cells in liquid.

The image of Fig. 6 demonstrates a fundamental difference with images obtained with conventional TEM. Whereas TEM usually addresses the cellular ultrastructure [46,47], sometimes with additional immuno-gold labeling, Liquid STEM highlights the labels but provides only low-resolution information of the ultrastructure. This difference is a direct consequence of the ability to image through the entire cell, in contrast to TEM of conventional thin sections. The lower-resolution analogy of Liquid STEM can be found in light microscopy, where fluorescence microscopy is used to study the locations of fluorescent labels nowadays with sub-diffraction resolution [48].

The electron dose amounted to 7×10^2 electrons/Å^2, an order of magnitude larger than the dose used for imaging frozen cells [46], and an order of magnitude smaller than that used for imaging conventional thin sections, for example, using STEM tomography [49]. Signs of sample damage were not observed when recording one or two images on the same area, but appeared after excessive imaging. The sample fixation thus provided sufficient stability to the sample, and the liquid flow presumably helped to remove free electrons, radicals, and heat produced by the impacting electron beam.

A percentage of 42% of the probe current was scattered into the ADF detector. Using Eq. (1), it was calculated that scattering amounted to a water thickness of 6 µm. It was thus concluded that the cells were completely covered in liquid. Note that this liquid coverage is not guaranteed using a system without liquid flow in the chamber. Gradual occurrence of gas bubbles was sometimes observed upon continuous imaging in other experiments using a completely sealed device [45]. In the latter case, a thin layer of liquid remained on the SiN window. The occurrence of bubbles was also reported by others [50] and appears to be the result of radiolysis of the water. Nevertheless, useful results can still be achieved for a thin liquid layer below a bubble, since the resulting liquid layer is very thin [25,45].

The sample preparation protocol is compatible with and as rapid as those of light microscopy [41]. Particularly useful is to combine light microscopy for overview images of the cells with Liquid STEM to localize the labels with nanometer precision via correlative fluorescence microscopy and Liquid STEM, for example, using quantum dot (QD)-labeled EGFRs [40].

5. Outlook on studying biological cells in liquid

Liquid STEM of a selected set of labeled molecules in fixed or live cells can be used for a wide variety of studies involving the functioning of cells at the molecular level. It is possible to determine the local stoichiometric distribution of protein complexes of, for example, the EGF receptor with relevance for cancer research. The distributions of monomers, dimers, and higher-order clusters can be analyzed as functions of cellular region for different experimental conditions. The results of several tens of cells can readily be collected [11], since there is no need for time-consuming sample preparation, such as thin sectioning. This type of experiment is expandable to a set of different proteins, using nanoparticle labels of different sizes, shapes, and materials.

A possible route towards optimizing the technology would be to adapt the STEM probe's convergence angle towards the minimal required resolution to resolve the nanoparticles. The data of Fig. 6a were recorded with a probe diameter of 1 nm, a pixel size of 0.91 nm, and a larger SNR than necessary to detect the label. A probe size of 5 nm in combination with a reduced probe current or pixel dwell time would be sufficient to detect the 10 nm AuNPs, and it can thus be expected that a reduction of the electron dose by at least a factor of 5^2 is possible. Much faster imaging seems also feasible. A technical difficulty is the need to refocus the STEM probe after shifting the sample, because the SiN window is bulged (curved) when

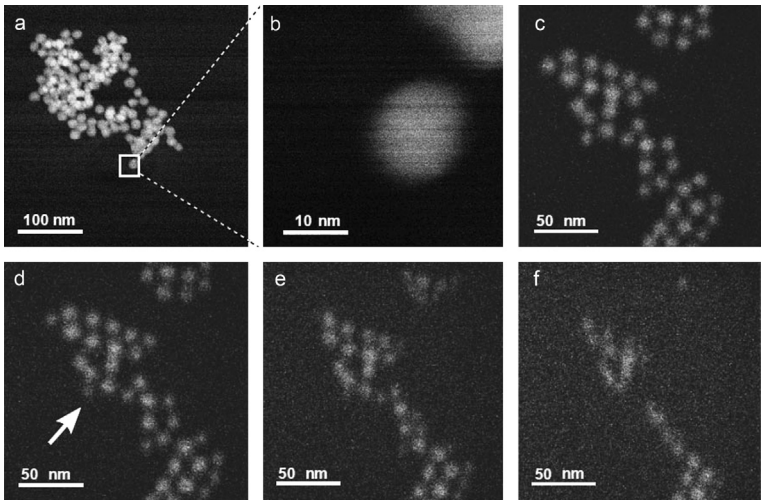

Fig. 7. AuNPs at the top of the water layer imaged with Liquid STEM. (a) Image of an AuNP cluster (magnification $M = 600{,}000\times$; pixel size $s = 370$ pm). (b) Focusing on the AuNP is indicated by the square in (a) ($M = 6{,}000{,}000\times$, $s = 37$ pm). Both images were recorded with a beam current $I = 80$ pA, a pixel dwell time of 5 µs, $E = 200$ keV, $\beta = 68$ mrad, and 1024×1024 pixels per image. (c–f) Pictures taken from a time-lapse image series showing several AuNPs disappearing due to the electron beam impact ($M = 1{,}200{,}000\times$).

placed in the vacuum chamber of the microscope, while electron dose needed for focusing should be minimized. A possible solution would be to adjust the focus according to the expected bending profile of the SiN [39].

First experiments also showed the feasibility of live cell Liquid STEM. COS7 cells can be kept alive in the microfluidics chamber for several hours. This allowed us to study the uptake of 30-nm-diameter AuNPs in live cells [51]. Other experiments involved correlative light microscopy and Liquid STEM on live yeast cells [42]. The ultimate goal is to study protein distributions in live cells via the recording of "snap shots" of molecular configurations of a selected set of macromolecules. We expect that the cells will start apoptosis *after* the recording of one image. Yet, this image will still reveal information from the natural state. The key idea is to study a group of cells first with light microscopy until a certain event or functional state of interest appears, after which the molecular configuration of a selected set of proteins is studied with Liquid STEM.

6. Liquid STEM of nanoparticles

Liquid STEM was also used to image AuNPs at the top of a water layer. The SiN windows were cleaned with acetone and ethanol to remove the resist [41]. They were made hydrophilic by exposure to O_2/Ar plasma for three minutes. A droplet of 0.5 µl of a water solution containing 15-nm-diameter AuNPs (24 mmol/l BBInternational) was pipetted on the SiN membrane using a micropipette (Eppendorf). This membrane became the top window on the inner side of the microfluidic cell after assembly. The liquid was dried in air, and the microchip was washed subsequently with water and ethanol to remove salt residues, while many AuNPs remained adherent to the SiN membrane. The microchip was then mounted in the liquid holder together with a second microchip with a 5-µm-thick spacer, and a droplet of 0.5 µl of pure water between the SiN membranes. A flow of pure water of 2 µl/min was applied to check for possible leaking or obstruction of the flow. Afterwards, the holder was transferred to the microscope (ARM200CF, JEOL) and the specimen imaged while a water flow was present in the liquid cell.

In Fig. 7a, a cluster of AuNPs is shown with a high contrast. The highlighted area was also imaged at a higher magnification (Fig. 7b) showing a single AuNP. To estimate the achieved resolution, we measured the 25–75% edge width d_{25-75} of a line scan (signal versus lateral position); the value amounted to 4.5 nm. To determine the thickness of the water, the percentage of electrons scattered into the ADF detector was measured [19,20]. It amounted to 28%, and using Eq. (1) it follows that $t = 3.3$ µm. The image was recorded at the edge of the SiN membrane, where bulging was much smaller than in the middle of the window. The measured thickness, however, was smaller than the spacer used (5 µm). The spacer for these microchips consisted of small pads at the corners of the microchips, and presumably, the microchips had bent as a result of the pressure on the O-rings. The resolution calculated using Eq. (7) for this thickness and amount of electrons per pixel amounts to 5.6 nm, slightly larger than the experimentally determined resolution. A higher resolution of up to one nanometer is possible at this liquid thickness for higher beam currents and/or pixel-dwell times [20].

At lower magnification ($200{,}000\times$), no influence of the electron beam on the imaging was noticed within several minutes. However, at a higher magnification of $1{,}200{,}000\times$, the interaction of the electron beam with the AuNPs led to a disappearance of several of the AuNPs from the window. To study this process in detail, a time-lapse image series was recorded via streaming continuously acquired STEM images with the Digital Video Capture in Digitalmicrograph (Gatan) using an image format of 640×480 pixels, and a frame interval of 30 ms. The streamed video was recorded by Windows Live Movie Maker. In Fig. 7c–f, several frames from the video are shown, i.e., those at 0 s, 23 s, 50 s, and 71 s, respectively.

The frames show the changes of the cluster of AuNPs with time. Both the spatial arrangement of the AuNPs changed, and the number of AuNPs decreased with time until all had vanished after 109 s (not shown). Surprisingly, the disappearance of the AuNPs was not an abrupt event. After 23 s, one of the NPs at the border of the cluster appeared blurred (arrow in Fig. 7d). It vanished after 50 s. At that time, most of the AuNPs appeared as blurred shapes. In Fig. 7e, almost all AuNPs lack a well-defined shape. A few frames later, all AuNPs disappeared from the field of view. One possible explanation of the blurry appearance can be the loosening from the SiN membrane, such that the AuNP started to move in the liquid but still remained loosely bound to the SiN membrane. Another possible explanation is the dissolution of the AuNP in water driven by local electric charge resulting from the interaction of the electron beam with the sample. To clarify this point, further experiments are needed.

The interactions of the electron beam with the liquid were also extensively discussed by others [50]. Heating of the liquid is not expected to have a significant effect on account of the small beam current and the good thermal conductance of water [52]. It appears that certain materials are attracted to the field of view in liquid while others, such as AuNPs, are repelled or disappear altogether. Series of quantitative experiments are needed to exactly understand the interactions of the electron beam with the specimen in the liquid. These experiments show that it is possible to achieve nanometer resolution in a liquid layer of 3.3 µm, while recording a movie in STEM mode.

The capability to image nanoparticles in liquid can be used to study growth [23] and self-assembly processes, and also to study movements of nanoparticles in liquids [25,37] at the nanoscale. In some cases, atomic resolution was achieved for the imaging of immobilized hydrated nanoparticles [23]. Interestingly, the movement of floating nanoparticles in close proximity of a SiN membrane was measured to be three orders of magnitude smaller than what would be expected for nanoparticles floating in a bulk liquid [25]. Thin liquid layers seem to exhibit much different flow behavior than bulk liquids.

7. Outlook on studying functional micro devices

The advantage of Liquid STEM to image through micrometers-thick liquid layers can readily be used to study the solid:liquid interface of nano- to micro-scale objects. The experimental setup provides some space to construct a functioning micro-device within the flow chamber. For example, pieces of battery material can be cut and deposited on a microchip using focused ion beam processing and micromanipulation. The microchips are available also with lithographically manufactured electrodes. Others have indeed studied lithium ion batteries using electron energy loss spectroscopy [27]. Another example would be to study the formation of hydrogen (nano) bubbles at electrodes in a liquid. The electrodes may also be configured as heating elements such that the microfluidic chamber could serve as a micro-reactor. One could then envision the study of the nanopores of deposited catalytic material during an actual catalytic reaction within the liquid. It would also be possible to cut micrometer-sized pieces of steel for the study of corrosion processes in situ. A wide variety of experiments can be designed [1]. The experiments, however, should be designed with great care. The ability to “see” at the nanoscale with the electron beam also introduces various changes to the object under observation. The electron beam impact causes the creation of free electrons (and radicals) in the liquid, electrolysis may occur at higher beam currents, leading to the formation of bubbles [45,50], and the sample may be heated, although the latter effect was calculated to be limited to several degrees Celsius only [52]. The experiments should at least be carried out at different electron doses so as to be able to separate beam-induced effects from the processes under observation [23,50].

8. Conclusions

Heavy nanoparticles are imaged with nanometer resolution in the top layer of a liquid of a light material by making use of the Z-contrast of ADF STEM. We derived an analytic equation of the resolution as a function of the sample thickness, the vertical position of a nanoparticle in the liquid, the properties of the involved materials, and the microscope settings. This equation may serve as a guide to design experiments and estimate expected resolution values. As nanoparticles are imaged deeper in the solution, the resolution gradually decreases and finally becomes limited by beam broadening. Tagged proteins can be imaged in a whole eukaryotic cell in liquid with relevance for biological research. Liquid STEM can readily be used to study gold nanoparticles in a liquid layer of up to ten micrometers. We have recorded time-lapse image series of gold nanoparticles moving in a water layer of 3.3-µm thickness. Gold nanoparticles were initially immobilized on the silicon nitride window, were detached under the influence of the electron beam at higher magnifications, and disappeared from the field of view. The capability of Liquid STEM to achieve nanoscale resolution in micrometer-thick liquid layers opens up new possibilities to investigate a wide variety of functional systems, e.g., whole cells, flowing nanoparticles, and micro-devices.

Acknowledgements

We thank Diana B. Peckys for discussions on biological imaging, and Protochips Inc., NC, USA for providing the Liquid STEM system. We thank E. Arzt for his support through INM. Research in part supported by NIH grant 2R44-EB008589 (to J. Damiano).

References

[1] N. de Jonge, F.M. Ross, Electron microscopy of specimens in liquid, Nat. Nanotechnol. 6 (2011) 695–704.

[2] E. Ruska, Beitrag zur uebermikroskopischen Abbildungen bei hoeheren Drucken, Kolloid-Z. 100 (1942) 212–219.
[3] M. von Ardenne, H. Friedrich-Freksa, Die Auskeimung der Sporen von Bacillus vulgatus nach vorheriger Abbildung im 200-kV-Universal-Elektronenmikroskop, Naturwissenschaften 35 (1941) 523–528.
[4] S.W. Hui, D.F. Parsons, Electron diffraction of wet biological membranes, Science 184 (1974) 77–78.
[5] M.J. Williamson, et al., Dynamic microscopy of nanoscale cluster growth at the solid–liquid interface, Nat. Mater. 2 (2003) 532–536.
[6] J.M. Yuk, et al., High-resolution EM of colloidal nanocrystal growth using graphene liquid cells, Science 336 (2012) 61–64.
[7] H. Zheng, et al., Observation of single colloidal platinum nanocrystal growth trajectories, Science 324 (2009) 1309–1312.
[8] K.L. Klein, I.M. Anderson, N. de Jonge, Transmission electron microscopy with a liquid flow cell, J. Microsc. 242 (2011) 117–123.
[9] A. Bogner, et al., Wet STEM: A new development in environmental SEM for imaging nano-objects included in a liquid phase, Ultramicroscopy 104 (2005) 290–301.
[10] D.L. Stokes, Principles and Practice of Variable Pressure/Environmental Scanning Electron Microscopy (VP-SEM), Wiley, Chichester, West-Sussex, 2008.
[11] D.B. Peckys, et al., Epidermal growth factor receptor subunit locations determined in hydrated cells with environmental scanning electron microscopy, Sci. Rep. 3 (2013) 2626.
[12] S. Thiberge, et al., Scanning electron microscopy of cells and tissues under fully hydrated conditions, Proc. Natl. Acad. Sci. USA 101 (2004) 3346.
[13] H. Nishiyama, et al., Atmospheric scanning electron microscope observes cells and tissues in open medium through silicon nitride film, J. Struct. Biol. 169 (2010) 438–449.
[14] N. de Jonge, et al., Scanning transmission electron microscopy of samples in liquid (liquid STEM), Microsc. Microanal. 13 (Suppl. 2) (2007) 242–243.
[15] A.V. Crewe, J. Wall, J. Langmore, Visibility of single atoms, Science 168 (1970) 1338–1340.
[16] S.A. Mueller, A. Engel, Biological scanning transmission electron microscopy: imaging and single molecule mass determination, Chimia 60 (2006) 749–753.
[17] L. Reimer, H. Kohl, Transmission Electron Microscopy: Physics of Image Formation, Springer, New York, 2008.
[18] C. Colliex, C. Jeanguillaume, C. Mory, Unconventional modes for STEM imaging of biological structures, J. Ultrastruct. Res. 88 (1984) 177–206.
[19] N. de Jonge, et al., Electron microscopy of whole cells in liquid with nanometer resolution, Proc. Natl. Acad. Sci. USA 106 (2009) 2159–2164.
[20] N. de Jonge, et al., Nanometer-resolution electron microscopy through micrometers-thick water layers, Ultramicroscopy 110 (2010) 1114–1119.
[21] Y. Xiao, et al., “Plugging into enzymes”: nanowiring of redox enzymes by a gold nanoparticle, Science 299 (2003) 1877–1881.
[22] J. Lippincott-Schwartz, E. Snapp, A. Kenworthy, Studying protein dynamics in living cells, Nat. Rev. Mol. Cell Biol. 2 (2001) 444–456.
[23] J.E. Evans, et al., Controlled growth of nanoparticles from solution with in situ liquid transmission electron microscopy, Nano Lett. 11 (2011) 2809–2813.
[24] E.R. White, et al., Charger nanoparticle dynamics in water induced by scanning transmission electron microscopy, Langmuir 28 (2012) 3695–3698.
[25] E.A. Ring, N. de Jonge, Video-frequency scanning transmission electron microscopy of moving gold nanoparticles in liquid, Micron 43 (2012) 1078–1084.
[26] K.L. Jungjohann, et al., Atomic-scale imaging and spectroscopy for in situ liquid scanning transmission electron microscopy, Microsc. Microanal. 18 (2012) 621–627.
[27] M.E. Holtz, et al., In situ electron energy-loss spectroscopy in liquids, Microsc. Microanal. 19 (2013) 1027–1035.
[28] J.E. Evans, et al., Visualizing macromolecular complexes with in situ liquid scanning transmission electron microscopy, Micron 43 (2012) 1085–1090.
[29] A. Engel, Molecular weight determination by scanning transmission electron microscopy, Ultramicroscopy 3 (1978) 273–281.
[30] A. Rose, Television pickup tubes and the problem of noise, Adv. Electron. 1 (1948) 131–166.
[31] D.C. Joy, C.S. Joy, Scanning electron microscope imaging in liquids – some data on electron interactions in water, J. Microsc. 221 (2005) 84–99.
[32] J.K. Hyun, P. Ercius, D.A. Muller, Beam spreading and spatial resolution in thick organic specimens, Ultramicroscopy 109 (2008) 1–7.
[33] A.A. Sousa, et al., Monte Carlo electron-trajectory simulations in bright-field and dark-field STEM: implications for tomography of thick biological sections, Ultramicroscopy 109 (2009) 213–221.
[34] J. Loos, et al., Electron tomography on micrometer-thick specimens with nanometer resolution, Nano Lett. 9 (2009) 1704–1708.
[35] H. Demers, et al., The probe profile and lateral resolution of scanning transmission electron microscopy of thick specimens, Microsc. Microanal. 18 (2012) 582–590.
[36] H. Demers, et al., Simulating STEM imaging of nanoparticles in micrometers-thick substrates, Microsc. Microanal. 16 (2010) 795–804.
[37] E.A. Ring, N. de Jonge, Microfluidic system for transmission electron microscopy, Microsc. Microanal. 16 (2010) 622–629.
[38] N. de Jonge, W.C. Bigelow, G.M. Veith, Atmospheric pressure scanning transmission electron microscopy, Nano Lett. 10 (2010) 1028–1031.
[39] M.E. Holtz, et al., In situ electron energy-loss spectroscopy in liquids, Microsc. Microanal. 19 (2013) 1027–1035.
[40] M.J. Dukes, D.B. Peckys, N. de Jonge, Correlative fluorescence microscopy and scanning transmission electron microscopy of quantum-dot-labeled proteins in whole cells in liquid, ACS Nano 4 (2010) 4110–4116.
[41] E.A. Ring, et al., Silicon nitride windows for electron microscopy of whole cells, J. Microsc. 243 (2011) 273–283.
[42] D.B. Peckys, et al., Fully hydrated yeast cells imaged with electron microscopy, Biophys. J. 100 (2011) 2522–2529.
[43] A. Arkhipov, et al., Architecture and membrane interactions of the EGF receptor, Cell 152 (2013) 557–569.
[44] N. Normanno, et al., Epidermal growth factor receptor (EGFR) signaling in cancer, Gene 366 (2006) 2–16.
[45] D.B. Peckys, et al., Nanoscale imaging of whole cells using a liquid enclosure and a scanning transmission electron microscope, PLoS ONE 4 (2009) e8214.
[46] A. Hoenger, C. Bouchet-Marquis, Cellular tomography, Adv. Protein Chem. Struct. Biol. 82 (2011) 67–90.
[47] L.F. Kourkoutis, J.M. Plitzko, W. Baumeister, Electron microscopy of biological materials at the nanometer scale, Annu. Rev. Mater. Res. 42 (2012) 33–58.
[48] J. Lippincott-Schwartz, S. Manley, Putting super-resolution fluorescence microscopy to work, Nat. Methods 6 (2009) 21–23.
[49] A.A. Sousa, et al., Dual-axis electron tomography of biological specimens: Extending the limits of specimen thickness with bright-field STEM imaging, J. Struct. Biol. 174 (2011) 107–114.
[50] T.J. Woehl, et al., Experimental procedures to mitigate electron beam induced artifacts during in situ fluid imaging of nanomaterials, Ultramicroscopy 127 (2013) 53–63.
[51] D.B. Peckys, N. de Jonge, Visualization of gold nanoparticle uptake in living cells with liquid scanning transmission electron microscopy, Nano Lett. 11 (2011) 1733–1738.
[52] H. Zheng, et al., Nanocrystal diffusion in a liquid thin film observed by in situ transmission electron microscopy, Nano Lett. 9 (2009) 2460–2465.